Remote sensing detection of altered zones associated with Cu-Mo mineralization in North of Zahedan, SE Iran using Landsat-8 data

Landsat-8 verileri ile Zahedan'ın kuzeyi, GD İran'da Cu-Mo cevherleşmelerine bağlı alterasyon zonlarının uzaktan algılama ile tespiti

RAHELE MORADI*, MOHAMMAD BOOMERI

*Department of Geology, Faculty of Sciences, University of Sistan and Baluchestan, Zahedan, Iran.

ABSTRACT

Hydrothermal alteration zones have highlighted role in prospecting mineral deposits. In this study and at the first stage, we used image processing techniques on the Landsat-8 image which covered the Lar area located in southeastern part of Iran. We applied the color composite, band ratio, Crosta and LS-Fit methods, high-pass directional filtering, and photolineament factor methods. The color composite and band ratio methods clearly showed the hydrothermal altered areas of clay minerals and iron oxides that are in compliance with the maximum amount of fractures. Both LS-Fit and Crosta methods enabled us to represent and acknowledge the altered hydroxyl and iron-oxide minerals in the study region. Finally, the high-pass directional filtering and photolineament factor methods were administered to map the geological structures and to determine the intense influences of hydrothermal fluids location. In the second stage, based on field observation, we managed to determine hydrothermal alterations as silicic, potassic, argillic, propylitic and phyllic without any normal zonation of porphyry deposits. Altered and mineralized area has an oval shape, with a NW-SE strike, mainly concentrated in the southwest of the Lar igneous complex. Mineralization often occurs in syenitic to monzonitic intrusions and in association with silicic veins and veinlets. Consequently, the results of image processing techniques showed high efficiency for mapping hydrothermal altered areas especially iron-oxide minerals which are alteration products of hydrothermal sulfides. These methods enabled us to identify the first Cu-Mo porphyry system in southeastern part of Iran before costly-detailed ground investigations.

Keywords: hydrothermal alteration mapping, Landsat-8, Crosta method, LS-Fit method, Lar Cu-Mo porphyry system, photolineament factor.

ÖZ

Maden yataklarının aranmasında hidrotermal alterasyon zonları önemli rol oynamıştır. Bu çalışmada ve öncelikle, İran'ın güneydoğusunda yer alan Lar bölgesinde Landsat-8 görüntüsü ile görüntü işleme teknikleri kullanılmıştır. Renkli karışım (color composite), band oranı, Crosta ve LS-Fit yöntemleri, yüksek geçiren filtreleme ve fotoçizgisellik yöntemleri kullanılmıştır. Renkli karışım ve band oranları kil ve demir oksit mineralli hidrotermal bozunma alanlarının en fazla kırıklanmanın olduğu zonlara karşılık geldiğini açıkça ortaya koymuştur. LS-Fit ve Crosta yöntemleri çalışma alanındaki hidroksil ve demir oksit minerallerinin yerlerinin saptanmasına yardımcı olmuştur. Sonuçta, yüksek geçiren filtre ve fotoçizgisellik yöntemleri jeolojik yapılarla hidrotermal akışkanların en yoğun olduğu zonların bulunmasında kullanılmıştır. İkinci aşamada, porfirik yataklarda bir anormal zonlanma göstermeyen silisik, potasik, arjillik, propilitik ve fillik hidrotermal bozunmaların saptanması ele alınmıştır. Bozunmuş ve mineralize olmuş alan KB-GD doğrultulu ve eliptik şekilli olup Lar magmatik karmaşığının güneybatısında zenginleşmiştir. Mineralizasyon sıklıkla silisli damar ve damarcıklara bağlı siyenitik ve monzonitic sokulumlara bağlıdır. Dolayısıyla görüntü işleme teknikleri özellikle hidrotermal sülfitlerin bozunma ürünleri olan demir oksit minerallerinin haritalanmasında çok etkili olmuştur. Bu yöntemler güneydoğu İran'da masraflı ayrıntılı yer çalışmaları öncesinde ilk defa Cu-Mo porfiri sisteminin saptanmasını sağlamıştır.

Anahtar Kelimeler: *hidrotermal bozunmanın haritalanması, Landsat-8, Crosta yöntemi, LS-Fit yöntemi, Lar Cu-Mo porfiri sistemi, fotoçizgisellik faktörü.*

---

* R.Moradi
e-posta: rmoradi@pgs.usb.ac.ir; rmoradi1391@gmail.com

INTRODUCTION

The Iranian plateau is part of the Alpine-Himalayas orogenic and metallogenic belt, which is one of the major structural features of the earth (Moores and Twiss, 1995). According to Berberian and King (1981) Iran is composed of several distinct geological tectonic zones (provinces) which are as follows: (1) Zagros Fold Belt, (2) Sanandaj-Sirjan Zone, (3) Sahand-Bazman Belt, (4) Central Iran, (5) Lut Block, (6) Alborz Zone, (7) Kopeh-Dagh zone, (8) Sistan suture zone (SSZ), (9) Makran zone. All zones are associated with the opening and closing of the Paleo-Tethys and Neo-Tethys oceanic basins due to subduction and collisional events in the northern to southern parts of Iran (Berberian and King, 1981).

The Lar Cu-Mo mineralization is geologically situated in the SSZ. The SSZ is a remnant of a Cretaceous oceanic basin that extends as a N–S trending belt over more than 700 km along the border between Iran, Afghanistan, and Pakistan. Generally, the SSZ igneous rocks are different in age, composition, and genesis and can be divided on the basis of age as follows: (1) Eocene calc-alkaline rocks of the accretionary prism that are attributed to subduction of the Lut block beneath the Afghan block (Camp and Griffis, 1982). (2) Early Oligocene Zahedan calc-alkaline I-, rare S-, and hybrid-type granitoids that are related to subduction and collisional events in the area (Camp and Griffis, 1982; Sahebzadeh, 1996; Hosseini, 2002; Boomeri et al., 2005; Kord, 2005; Sadeghian, 2005; Sadeghian et al., 2005; Sadeghian and Valizadeh, 2007; Rahnama-Rad et al., 2008; Ghasemi et al., 2010; Moradi et al., 2014; Mohammadi et al., 2016). (3) Oligocene to Middle Miocene alkaline and calc-alkaline igneous rocks between the cities of Zahedan and Nehbandan (Camp and Griffis, 1982). (4) Quaternary volcanic rocks like Mount Taftan that are related to the Makran active subduction of the Oman oceanic lithosphere under the Makran zone and the SSZ (Farhoudi and Karig, 1977).

Furthermore, the Lar Cu-Mo mineralization is geographically located in 20 km north of Zahedan, southeast of Iran, adjacent to the Iran and Pakistan border and close to the Saindak and giant Reko Diq copper deposits of Pakistan (Figure 1). This mineralization was formed in the western and southwestern part of an intrusive-extrusive igneous complex named Lar mountain or the Lar igneous complex (LIC). Although the LIC has been subject of several petrolo-

gical and geochemical studies (Chance, 1981; Bagheri and Bakhshi, 2001; Nakisa, 2002; Karimi, 2002; Boomeri, 2004; Ghafari-Bijar, 2009; Farokh-Nezhad, 2011; Soltanian, 2013), remote sensing studies have not previously been performed in the Lar Cu-Mo mineralization and associated hydrothermal alterations. Moreover, the Lar area has great potentials for mineral explorations such as Cu, Mo, and Au concerning some enormous copper reserves that are located in Pakistan (like Saindak and Reko Diq).

Many ore deposits are first detected in the field by the recognition of hydrothermally altered host rocks and remote sensing studies are applicable in recognizing hydrothermally altered rocks and exploration of many ore deposits like epithermal gold, porphyry copper, massive sulfide and uranium deposits (Daneshfar et al., 2006; Madani, 2009; Shalaby et al., 2010; Pour and Hashim, 2013; Ciampalini et al., 2013; Pour and Hashim, 2014; Pour et al., 2014; Ali and Pour, 2014; Pour and Hashim, 2015a, 2015b, 2015c; Zhang et al., 2016; Safari et al., 2017; Gahlan and Ghrefat, 2017). Since the main purpose of image processing in the Lar area is the recognition of alteration and related lineaments to the mineralization; therefore, the processing methods were selected in such a way that the spectral responses of the hydrothermal alteration index minerals become more identifiable in outcrops. Among the various methods, we used color composite, band ratio, both Crosta and LS-Fit methods, high-pass directional filtering, and photolineament factor to map the lithological unites, hydrothermal alterations (i.e. clay minerals and iron oxides), and geological structures. Application of these methods in the Lar area can help achieve better results regarding exploration of mineralized zones. In addition, this area has arid and semi-arid climate; therefore, using the multi-spectral images of Landsat is highly effective in hydrothermal alteration mapping. As a result, these investigations set a goal to acquire comprehensive and accurate information to explore the potentially interesting areas of Cu-Mo mineralization using Landsat data. Finally, geological survey was carried out to check the results of remote sensing with the geological reality of the Lar area.

Lithological units of the mineralized area

The Lar Cu-Mo mineralization geology consists of flysch and volcanic rocks intruded by syenitic to monzonitic rocks. The northeastern and eastern parts of
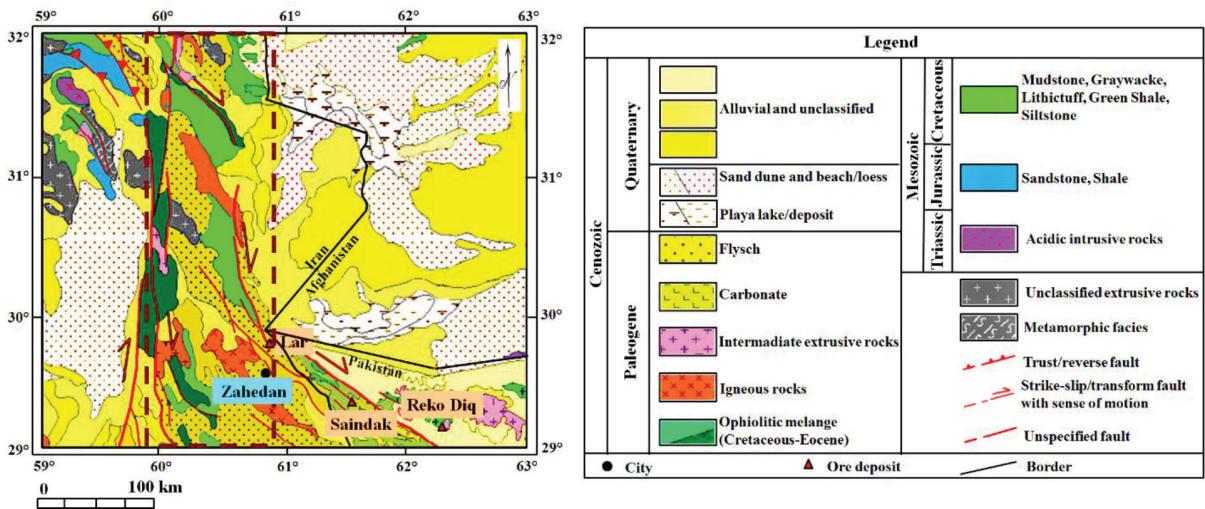
Figure 1. Location map of the Lar Cu-Mo mineralization (Based on geological map of Middle East 1:5000000 from Haghipour et al., 2009). The red dashed rectangle represents the SSZ (Sistan suture zone).

Şekil 1.   Lar Cu-Mo yatağının bulduru haritası (1:5000000 ölçekli Orta Doğu jeoloji haritasından, Haghipour et al., 2009). Kırmızı kesikli çizgili dikdörtgen Sistan kenet zonunu (SSZ) göstermektedir.

the mineralized area consist of unaltered intermediate igneous rocks and its southwestern and western parts consist of the flysch-type rocks (Figure 2).

MATERIAL and METHODS

Data analysis and image pre-processing

In general, satellite remote sensing images have widely and successfully been used for mineral exploration since the launch of Landsat in 1972 (Abdelsalam and Stern, 2000; Carranza and Hale, 2002; Daneshfar et al., 2006; Madani, 2009; Pour and Hashim, 2011a, 2011b; Pour and Hashim, 2012a, 2012b; Ciampalini et al., 2013; Ali and Pour, 2014; Zhang et al., 2016; Ducart et al., 2016; Safari et al., 2017; Gahlan and Ghrefat, 2017; Masoumi et al., 2017). Landsat-8 also was also launched on February 4th, 2013 from Vandenberg Air Force Base in California. It is an American Earth observation satellite and joins Landsat-7 on-orbit, providing increased coverage of the Earth's surface. It is a free-flyer spacecraft carrying two sensors: the Operational Land Imager (OLI) and the Thermal Infrared Sensor (TIRS). These two instruments collect images for nine visible near-infrared, and shortwave infrared bands, and two long-wave thermal bands. They have high signal-to-noise radiometer performance, allowing 12-bit quantification of data, thus providing more bits for better land-cover characterization. Landsat-8 provides

moderate-resolution imagery from 15 to 100 m of the Earth's surface and Polar Regions (US Geological Survey, 2012; Pour and Hashim, 2015a).

In this study, image processing techniques were applied using ENVI 4.5 and ArcGIS 10. A scene of Landsat-8 data (path 157, row 39) including the Lar area is used for this study. To obtain more accurate information, pre-processing such as geometric and radiometric corrections were performed by ENVI 4.5. Geometric correction has been performed using ground control points from topographic sheets. The root mean square error (RMS) in the geometric processing was less than one pixel.

Image processing methods

In general, selection of the best color composite images is useful for extracting meaningful information about the lithologies and alteration zones in ore mineral exploration. Band ratio technique is one of the most applicable techniques used to detect the hydrothermal alteration minerals such as clay, alunite, and iron minerals (Goetz et al., 1983; Sabins, 1999; Di Tommaso and Rubinstein, 2007).

The band ratio method is used to reduce the brightness of the sun, topography, and spectral data detection in images (Gupta, 2003). The selection of the bands being used in the development of band ratio images depends on the analysis of spectral charac-
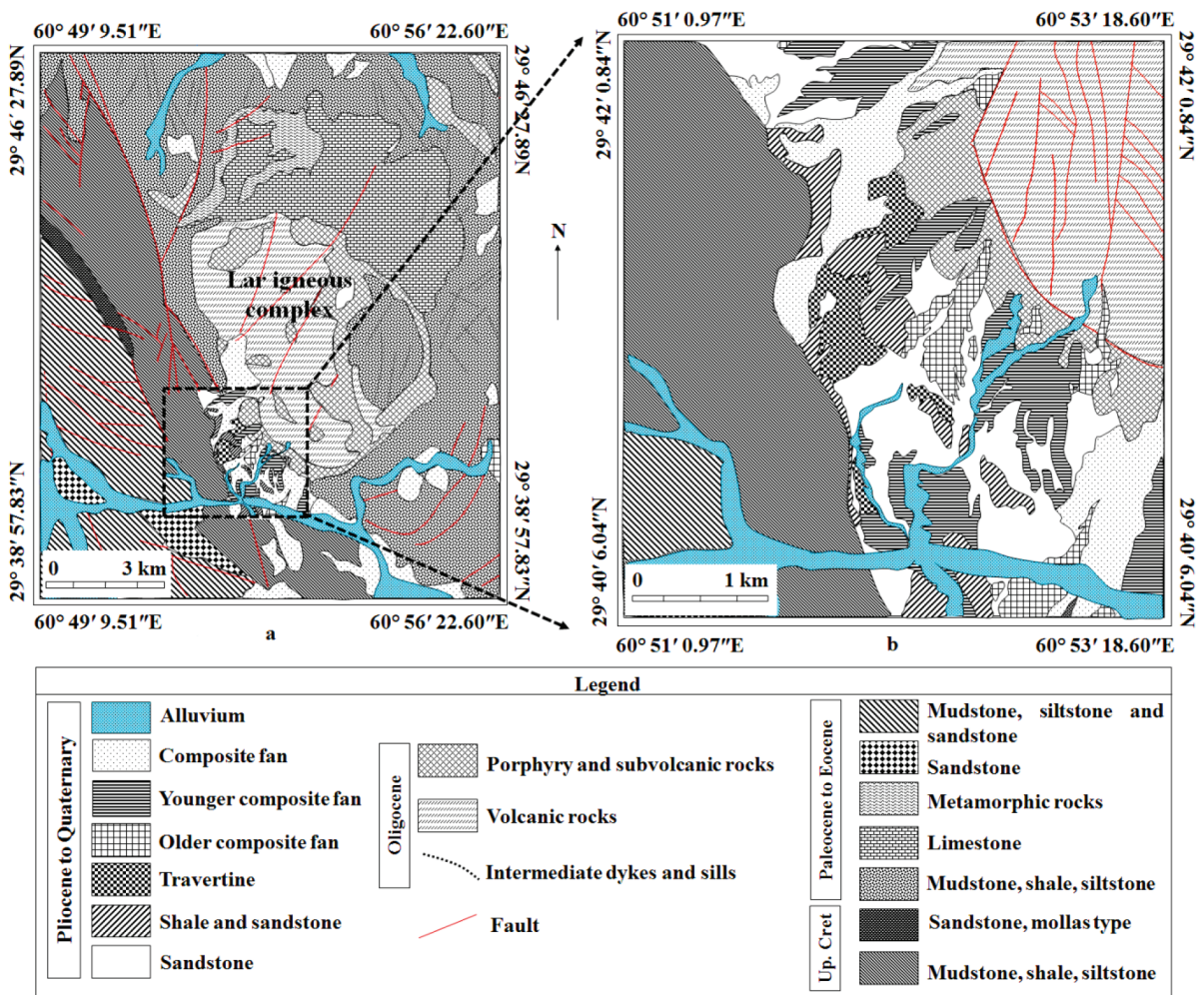
Legend

Pliocene to Quaternary		Oligocene		Paleocene to Eocene	
Alluvium		Porphyry and subvolcanic rocks		Mudstone, siltstone and sandstone	
Composite fan		Volcanic rocks		Sandstone	
Younger composite fan		Intermediate dykes and sills		Metamorphic rocks	
Older composite fan		Fault		Limestone	
Travertine				Mudstone, shale, siltstone	
Shale and sandstone				Sandstone, mollas type (Up. Cret)	
Sandstone				Mudstone, shale, siltstone	

Figure 2. (a) Regional geological map of the Lar area (Based on Behrouzi, 1993), (b) Geological map of the Lar Cu-Mo mineralization (modified from Kan Iran Engineering, 1999).

Şekil 2. a) Lar alanının bölgesel jeoloji haritası (Behrouzi, 1993'den) b) Lar Cu-Mo yatağının jeolojik haritası (Kan Iran Engineering, 1999'dan değiştirilerek).

teristics of the surface material and the abundance of this material is associated with the surroundings (Thurmond et al., 2006).

Crosta method is widely used for mapping alteration zones containing iron oxides and clay matrixes with hydroxyl ions content in metallogenic provinces (Abrams et al., 1997; Kaufman, 1988; Loughlin, 1991; Bennett et al., 1993; Tangestani and Moore, 2001; Crosta et al., 2003; Ranjbar et al., 2004; Amer et al., 2010; Pour and Hashim, 2013). This technique was proposed for the first time by Crosta and Moore (1989), in order to indicate a specific purpose as lighter pixels than the other phenomenon in one of the principal component images. This technique indicates whether the materials are represented in bright or dark pixels in the principal components according

to the magnitude and the sign of the eigenvector loadings. This technique can be applied on four bands of Landsat-8 data (Ali and Pour, 2014; Zhang et al., 2016; Ducart et al., 2016; Safari et al., 2017; Gahlan and Ghrefat, 2017; Masoumi et al., 2017).

LS-Fit method was used to map spectral signatures of hydrothermal alterations (i.e. clay minerals and iron oxides). This method performs a linear band prediction using least squares fitting technique. It calculates the covariance of the input data and uses it to predict the selected band as a linear combination of the predictor bands (Haroni and Lavafan, 2007).

RESULTS AND DISCUSSIONS

Landsat-8 image processing

Color composite

Digital images have been displayed as additive color composite. Different spectral bands of Landsat-8 data have been combined in RGB color system to make color composite images (Crosta and Moore, 1989). In the area under consideration, color composite of Landsat-8 bands 6, 4, 2 and 10, 7, 2 displayed the best band combination for the identification of rock types and alteration areas respectively (Figures 3 and 4).

By comparing of figures 2 and 3, the major lithologies could be separated, showing the main lithological units in the Lar area including igneous rocks, siliciclastic (flysch) rocks, travertines, and main focus of alteration areas in northwestern part of the igneous rocks. The flysch type rocks also could be recognized by their bedding forms in western part of the area in (Figure 3). At the same time, Figure 4 shows another RGB image which enabled us to determine silicic areas as pink color. It is clearly observed that

the silicic alteration is the most dominant alteration in the Lar area.

Band ratio

In General, hydroxyl-bearing minerals are from the most widespread products of alteration. An abundance of clays and sheet silicates implies that high absorption is in Band 7 and a very high reflectance in Band 5 (Rowan et al., 1977; Sabins, 1997; Drury, 2001); therefore, a band ratio of 5/7 would yield very high values for altered zones comprising dominantly hydroxyl-bearing minerals. This feature of phyllosilicates has been used in numerous mineral exploration investigations (Ranjbar et al., 2004). Using this ratio leads to a better recognition of the clay minerals as light tone in the study area (Figure 5). Iron oxide minerals (such as limonite, goethite, and hematite) are also quite a common constituent of alteration zones associated with hydrothermal sulphide deposits which have reflectance maxima within Landsat-8 band 4 and reflectance minima within Landsat-8 band 1. Hence, the iron oxide-bearing minerals can be detected by the band ratio of 4/2. Applying this ratio leads to a better distinction between hydrothermally altered and unaltered rocks as light tone in
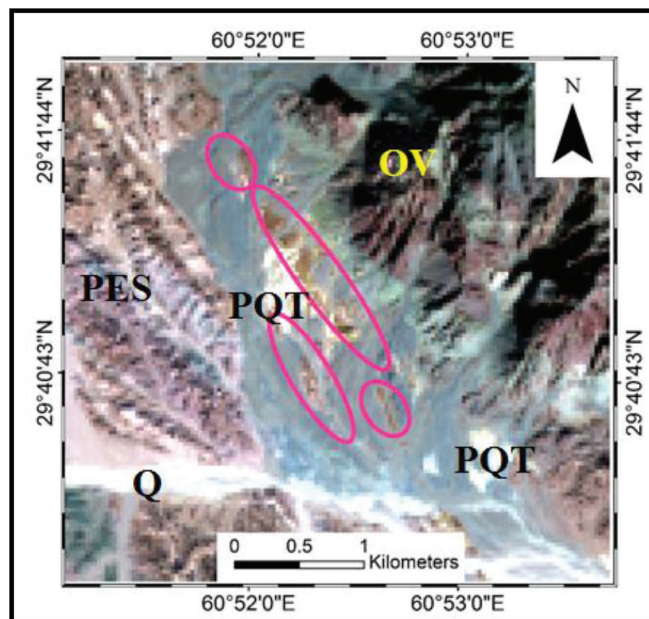

Figure 3. Color composite of the Lar mineralized area (RGB 6: 4: 2); PES: Paleocene to Eocene siliciclastic rocks, OV: Oligocene volcanic rocks; PQT: Pliocene to quaternary travertine, Q: Quaternary alluvial plains, ellipses: iron oxides.

Şekil 3.   Lar yatağının renk karışım haritası (RGB 6: 4: 2); PES: Paleosen-Eosen silisiklastik kayaçları; OV: Oligosen volkanik kayaçları; PQT: Plio-Kuvaterner traverten; Q: Kuvaterner alüvyon; elipsler: demir oksitler.
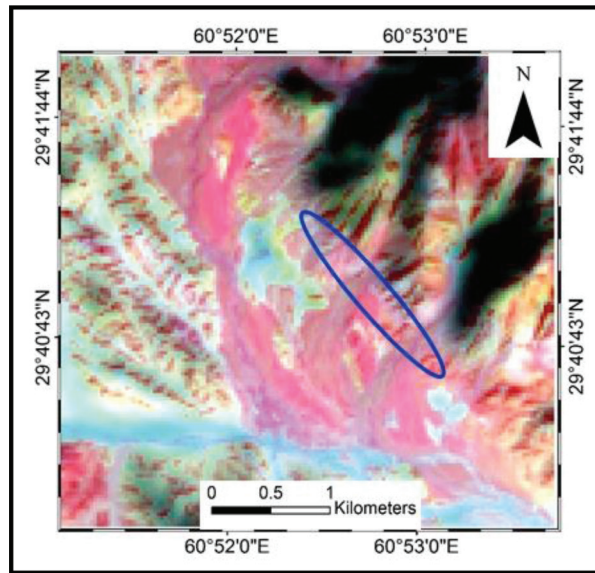
Figure 4. Color composite of the Lar mineralized area (RGB 10: 7: 2) for determination of silicic area as pink color.
Şekil 4.   Lar yatağında pembe renkte gösterilen silisli bölgenin saptanması için kullanılan renk karışımı (RGB 10: 7: 2) haritası.
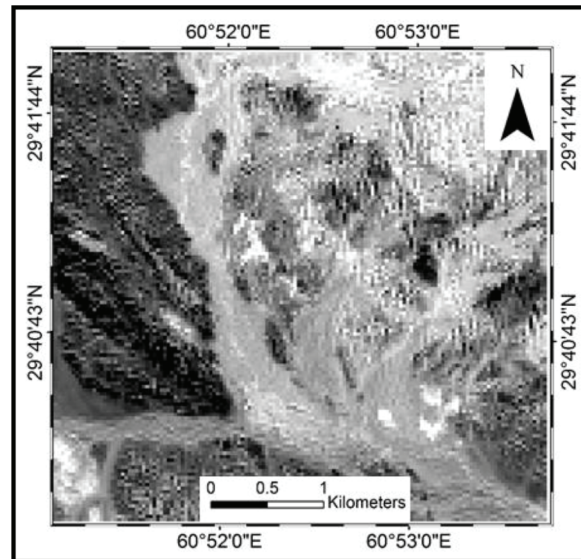

Figure 5. Landsat-8 band ratio (5/7) image of the Lar mineralized area. Areas with abundant hydroxyl-bearing minerals are shown as bright pixels.
Şekil 5.   Lar yatağında Landsat-8 band oranı (5/7) haritası. Parlak pikseller yoğun hidroksilli minerallere karşılık gelmektedir.

the present area (Figure 6). Also, obtained false color composite image shows hydroxyl-bearing and iron oxide areas as brownish and yellowish color respectively (Figure 7).

Crosta method (Selective principle component analysis)

The principal component transformation (eigenvectors and eigenvalues), described in Table 1, is perfor-

med using four bands of Landsat-8 as input bands (bands 3, 5, 6, and 7). The component of PC2 (Table 1) indicates that the clay minerals have high absorption in band 7 and high reflection in band 5. Therefore, pixels that have hydroxyl minerals will be lighter in the final hydroxyl image (Figure 8). The same technique is used on four bands of Landsat-8 (Bands 2, 3, 4, and 6) to enhance iron oxides. According to Table 2, iron oxide minerals have strong absorption feature in band 4 and strong reflection in band2. These two
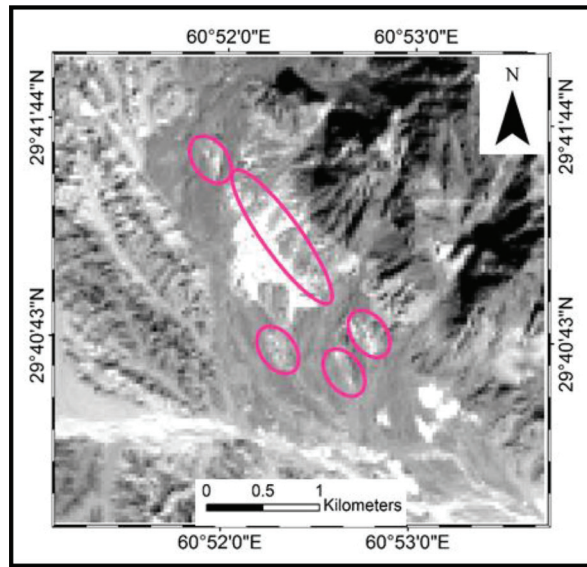
Figure 6. Landsat-8 band ratio (4/2) image of the Lar mineralized area. Areas with abundant iron oxide minerals are shown as bright pixels.
Şekil 6.   Lar yatağında Landsat-8 band oranı (4/2) haritası. Parlak pikseller yoğun demir oksitli minerallare karşılık gelmektedir.
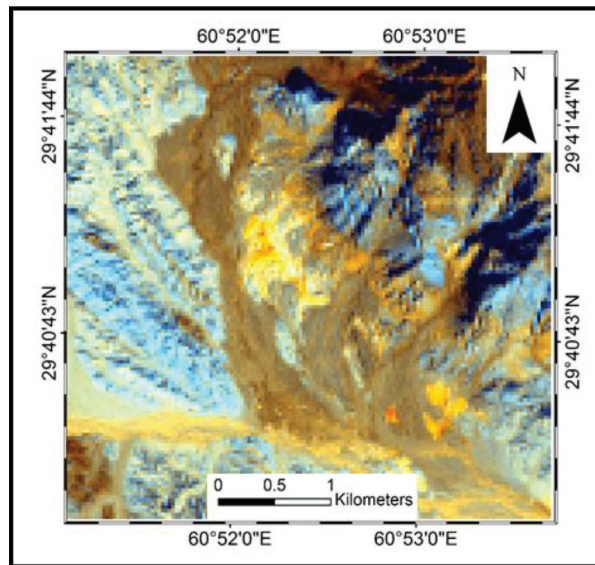

Figure 7. False color composite image (RGB) of iron oxide image (red), hydroxyl image (blue) and the average of these two images (green) showing hydroxyl-bearing minerals as brownish color and iron oxide minerals as bright to yellowish colors.
Şekil 7.   Sahte renklendirilmiş (RGB) demir oksit (kırmızı) görüntüsü, hidroksil (mavi) görüntüsü ve bu iki görüntünün ortalaması (yeşil), hidroksilli mineralleri kahverengi, demir oksitli mineralleri ise sarımsı veya parlak renklerde göstermektedir.

bands have therefore higher loadings through PC3 analysis and the pixels with more iron oxide mineral abundant would turn out lighter in the final image (Figure 9). To gain better examination, we used a false color composite image in which hydroxyl-bearing minerals and iron oxide minerals are shown as bright and dark blue colors, respectively (Figure 10).

Table 1.   Eigenvalues calculated for principal components of data for hydroxyl-bearing minerals on four bands of Landsat-8.

Çizelge 1. Landsat-8 dört bandında hidroksilli minerallerin ana bileşenleri için hesaplanan aygen değerleri.

	Band3	Band5	Band6	Band7
PC1	0.288	0.463	0.632	0.549
PC2	0.377	0.748	-0.419	-0.347
PC3	0.530	-0.295	-0.535	0.586
PC4	0.702	-0.369	0.371	-0.482
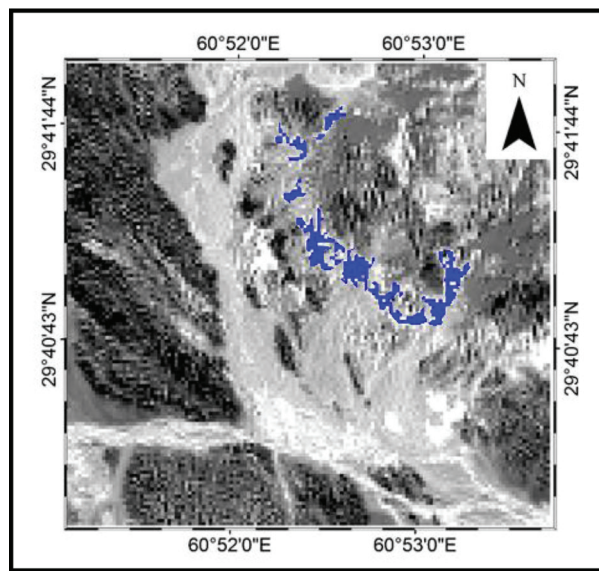
Figure 8. PC2 image of the hydroxyl-bearing minerals. Areas with abundant hydroxyl-bearing minerals are shown as blue pixels.

Şekil 8.   Hidroksilli minerallerin PC2 görüntüsü. Yoğun hidroksilli mineral alanları mavi pikseller olarak görülmektedir.

Table 2.   Eigenvalues calculated for principal components of data for iron oxide minerals on four bands of Landsat-8.

Çizelge 2. Landsat-8 dört bandında demir oksitminerallerin ana bileşenleri için hesaplanan aygen değerleri.

	Band2	Band3	Band4	Band6
PC1	0.238	0.355	0.473	0.769
PC2	0.369	0.427	0.526	-0.635
PC3	-0.679	-0.309	0.662	-0.054
PC4	0.587	-0.771	0.243	0.024

LS-Fit method

We used this method to map spectral signatures of hydrothermal alterations (i.e. clay minerals and iron oxides), presented in Figures 11 to 13. Figure 11 illustrates an output image of the LS-Fit met-

hod indicating the distribution of clay alterations (hydroxyl-bearing minerals) as blue pixels. This map was created using two bands of 7 and 5. This method was also applied to find the iron-oxidations due to its association with hydrothermal alterations. In
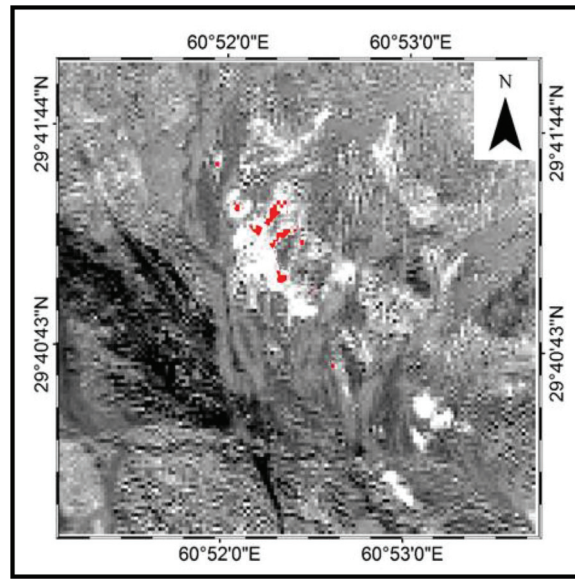
Figure 9. PC3 image of the iron oxide minerals. Areas with abundant iron oxide minerals are shown as red pixels.
Şekil 9.   Demir oksitli minerallerin PC3 görüntüsü. Yoğun demir oksitli mineral alanları kırmızı pikseller olarak görül-mektedir.
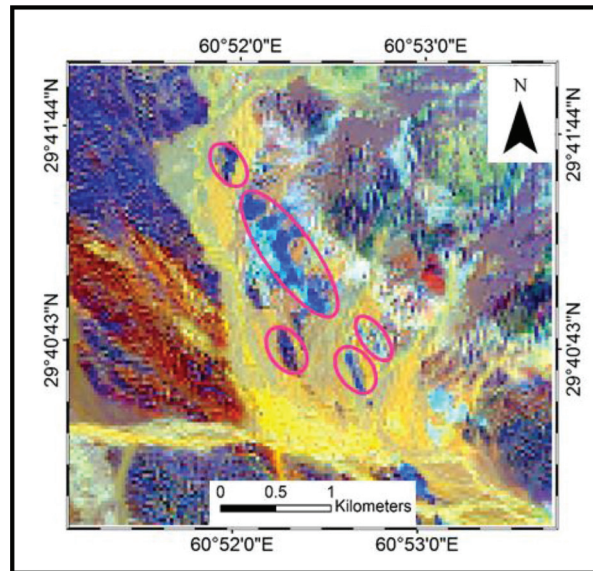

Figure 10. PCA false color composite image of Landsat-8 (RGB: PC3, PC3+PC2, PC2) showing hydroxyl-bearing minerals as bright pixels and iron oxide minerals as pink ellipses.
Şekil 10.   Landsat-8 PCA sahte renkli görüntüsü (RGB: PC3, PC3+PC2, PC2) hidroksilli mineralleri parlak, demir oksitli mineralleri ise pembe elipsler olarak göstermektedir.

this case, iron oxides show as red pixels that were created using two bands of 4 and 2 (Figure 12). For closer examination, we used a false color composite image of Landsat-8 by LS-Fit method. In this image, hydroxyl-bearing minerals and iron oxides are shown as yellow and light blue pixels respectively (Figure 13). Moreover, travertines are more highlighted as white pixels.

High-pass directional filtering

In general, lineaments are not readily detectable on satellite images. Some of them are more easily recognized, according to the lighting conditions, the presence of vegetation, and waterways; but other complications could be revealed with image processing techniques. To clarify these lineaments, we
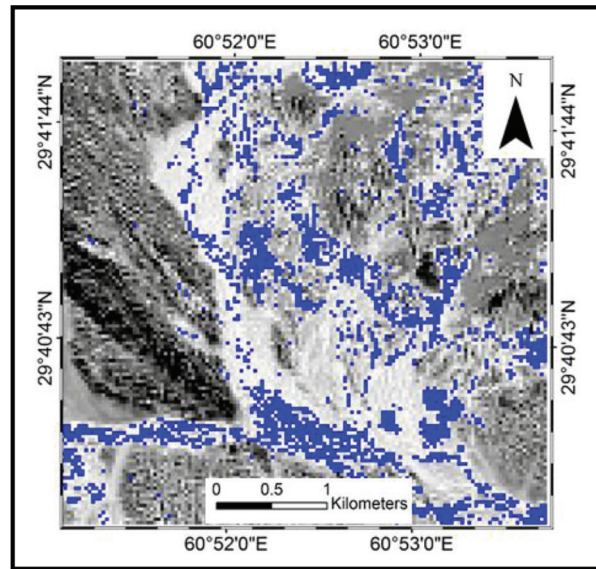
Figure 11. LS-Fit image of the Lar area show hydroxyl-bearing minerals as blue pixels.
Şekil 11.   Lar yatağının hidroksilli minerallerini mavi pikseller şeklinde gösteren LS-Fit görüntüsü.
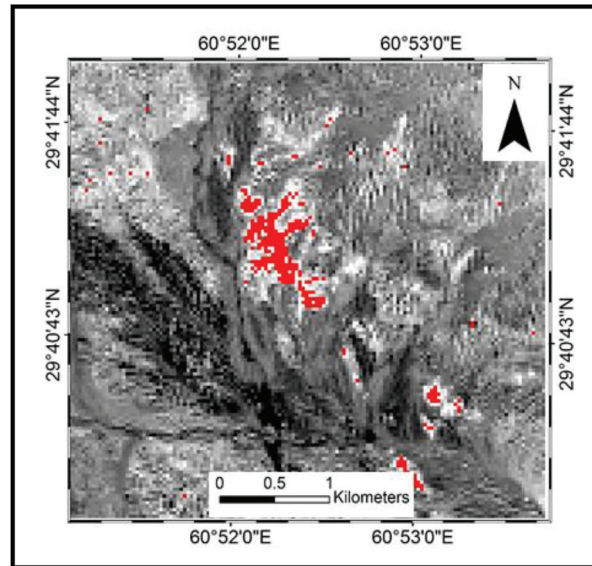

Figure 12. LS-Fit image of the Lar area show iron oxides minerals as red pixels.
Şekil 12.   Lar yatağının demir oksitli minerallerini kırmızı pikseller şeklinde gösteren LS-Fit görüntüsü.

have to use special filtering. Although, there are several ways to filtering, directional and non-directional are more applicable filters. In this study, we used high-pass directional filtering (Table 3 and Figures 14 to 17), since directional filters can be used to detect lineaments with particular trends and they are applied in the study of geological lineaments. Generally, numbers in the cornell are selected in such a way that the lineaments become clearer in a specific

direction (Table 3).

The full color band of Landsat-8 has been used to enhance the lineament. As Wester (1992) suggested, filtered images (using above directional filters) are combined with each other and obtained images are transferred to the RGB systems. Then elongation differentiation was performed and lineaments in N-S, E-W, NW-SE, and NE-SW directions were cle-
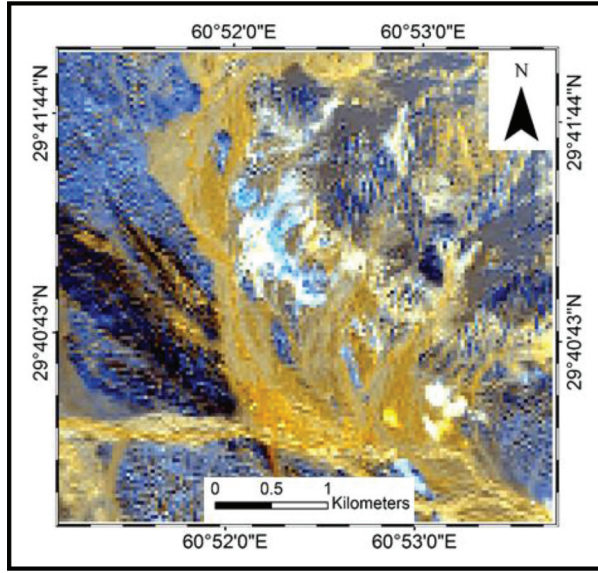
Figure 13. False color composite image (RGB) of hydroxyl image (red), iron oxide image (blue) and the average of these two images (green) by LS-Fit method. Hydroxyl-bearing minerals, iron oxide minerals, and travertines are shown as yellow, light-blue, and white colors respectively.

Şekil 13. LS-Fit yöntemi ile elde edilen hidroksil görüntüsü (kırmızı), demir oksit görüntüsü (mavi) ve bu iki görüntünün ortalaması (yeşil). Hidroksilli mineraller sarı, demir oksitli mineraller açık mavi ve travertenler beyaz renkte görülmektedir.

Table 3.   Direction filters of Landsat-8 in the Lar mineralized area.

Çizelge 3. Lar yatağında Landsat-8 doğrultu filtreleri.

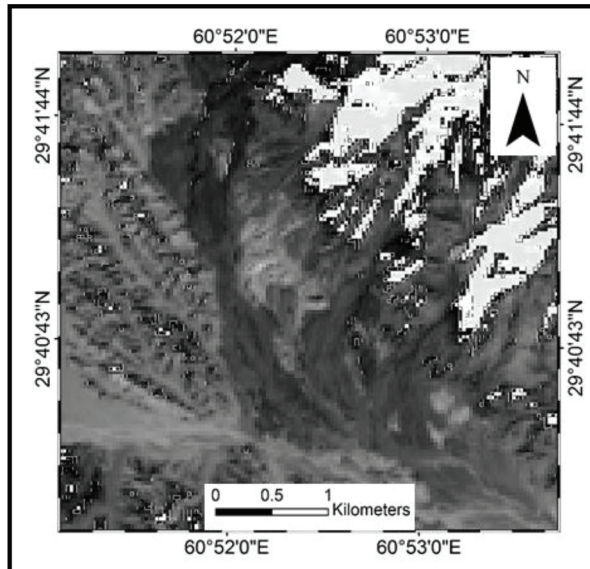| N-S			E-W			NW-SE			NE-SW		
-1	1	-1	-1	-1	-1	1	-1	-1	-1	-1	1
-1	4	-1	1	4	1	-1	4	-1	-1	4	-1
-1	1	-1	-1	-1	-1	-1	-1	1	1	-1	-1

Figure 14. N-S directional filtering of Landsat-8 in the Lar mineralized area.

Şekil 14.   Lar yatağı için Landsat-8 görüntüsünde K-G doğrultulu filtreleme.
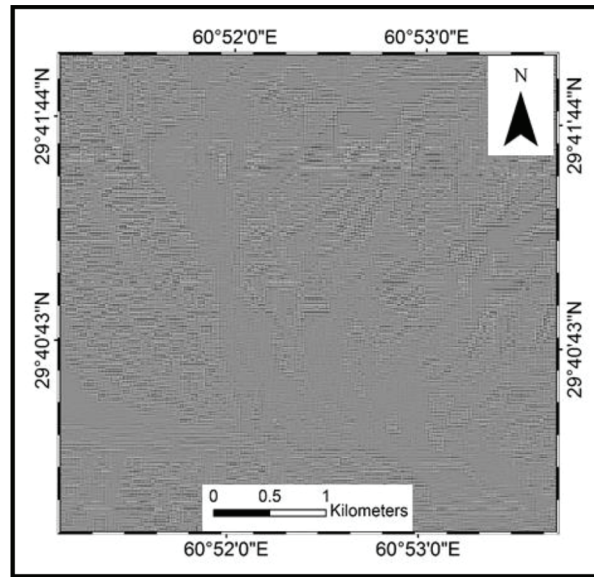
Figure 15. E-W directional filtering of Landsat-8 in the Lar mineralized area.
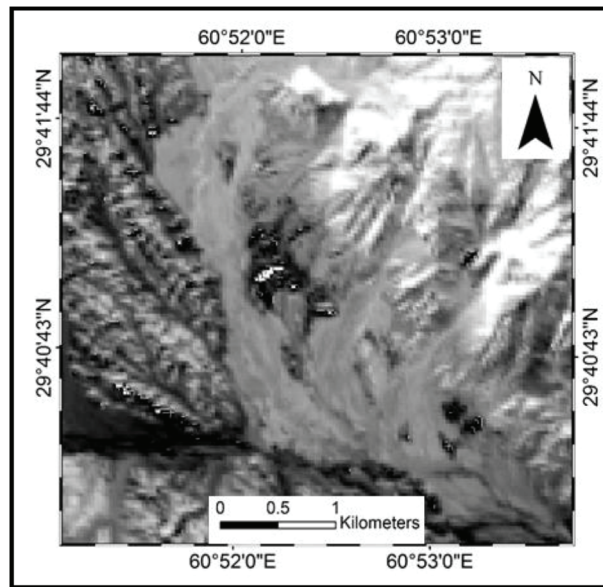*Şekil 15.   Lar yatağı için Landsat-8 görüntüsünde D-B doğrultulu filtreleme.*

Figure 16. NE-SW directional filtering of Landsat-8 in the Lar mineralized area.
Şekil 16.   Lar yatağı için Landsat-8 görüntüsünde KD-GB doğrultulu filtreleme.

arer on the obtained image. Eventually, lineaments were drawn using these image on the whole of the Lar area (Figure 18). Now, it is possible to use this image for lineaments analyses and rose diagramming as below:

There are abundant lineament systems in area under consideration which are related to the tectonic events of the s. In general, two dominant directions of linea-ments can be easily identified as NW-SE and NE-SW in Figures 18 and 19. Based on Figure 18, NE-SW striking is composed of continuous lineaments in the central to eastern and the NW-SE striking focuses on the central and western part of the image where the latter is in accordance with the Zahedan faulting system. Moreover, associated lineaments with streams are interpreted to be fault controlled.
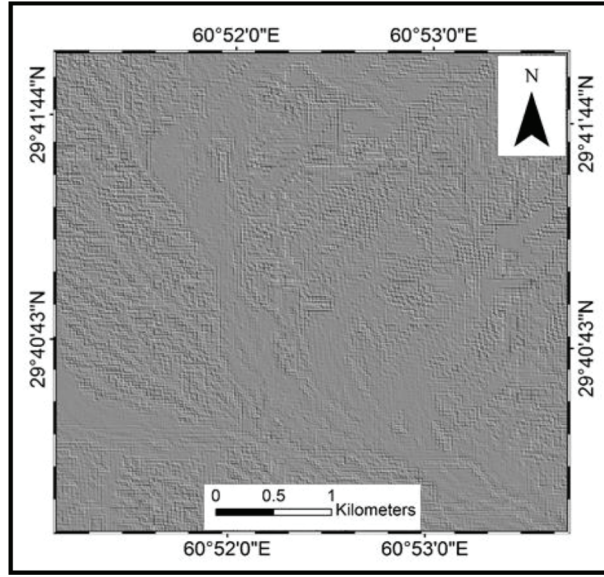
Figure 17. NW-SE directional filtering of Landsat-8 in the Lar mineralized area.
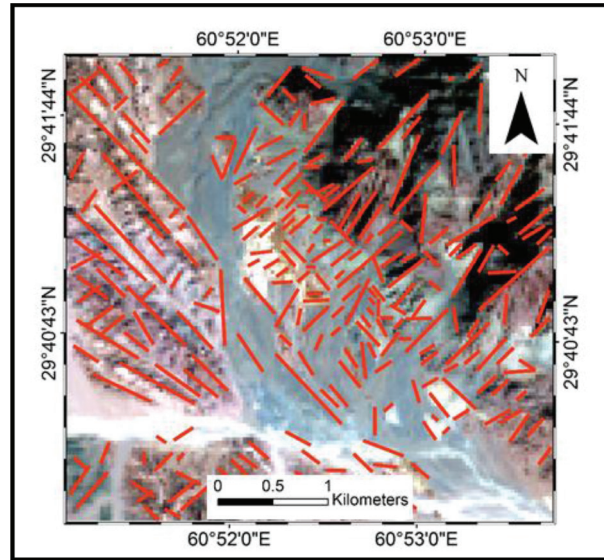*Şekil 17.   Lar yatağı için Landsat-8 görüntüsünde KB-GD doğrultulu filtreleme.*

Figure 18. Interpreted lineaments from directional filtering images in the Lar mineralized area.
Şekil 18.   Lar yatağı için doğrultu filtrelerinden itibaren yorumlanan çizgisellikler.

Photolineament factor

Photolineament factor or PF is another method that could be used for lineaments analysis. This method is often applicable to explore groundwater and mineral resources in crushed rocks. Lineaments are associated with areas that bedrocks have a lot of fractures. In general, these fractures are capable to store and transfer large volumes of groundwater and hydrothermal fluids. Calculation of photolineament factor and spatial distribution studies of lineaments

are beneficial in ore mineral exploration and determination of the water storage and transfer areas. In this method, parameters such as the number, lengths, intersections, and directions of fractures have been used for fracture analysis by the following equation (Hardcastle, 1995): $PF = (a/A) + (b/B) + (c/C) + (d/D)$.

A suitable cellular network was considered for lineaments analysis and was plotted on the photolineament map and above formula parameters were separately derived in each cell where *a* is the number
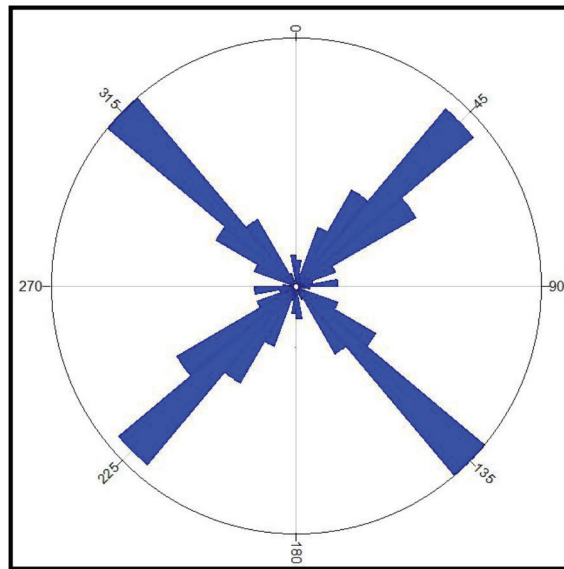
Figure 19. Rose diagram by dominant trends of lineaments in the Lar mineralized area.
Şekil 19.   Lar yatağı için hâkim çizgisellik doğrultularının gül diyagramı.

of fractures in each cell; *A* is the average in each map; *b* is fracture length in each cell; *B* is the average in each map; *c* is the number of fractures intersection in each cell; *C* is the average in each map; *d* is the number of direction sets in each cell; and *D* is the average in each map. Then lineation contour map was prepared with obtained values from above equation in ArcGIS10 (Figure 20). Based on lineation contour map, the mineralized and altered areas are in compliance with high values of photolineament factor.

Field Observations

According to the field observations (Figure 21), associated hydrothermal alteration to the Lar mineralization is mainly concentrated in the southwestern part of the Lar igneous complex with NW-SE direction. The alterations are often associated with tectonics and they are more intense in direction of the main fault zone. On the other hand, tectonics play a significant role in the control of alteration and mineralization focuses. Lateral extension of the alteration has not been widespread and it had only small effects around the fractures. Altered area is associated with iron bearing areas. Generally, usual alteration zoning which can be seen in the porphyry copper deposits has not been formed in this area. According to the microscopic sections, secondary potassium feldspar and biotites which form respectively from pla-

gioclase and amphiboles breakdown are frequently observed. These phenomena suggest the existence of potassic alterations. Nevertheless, the Lar deposit rocks are high in potassium feldspar, but the remnants of poly-synthetic twining of plagioclase can be seen. Most of the ore zone lies within potassically altered rocks and syenites. The other minor alterations are propylitic, phyllic, and argillic (Figures 22- a to e). The Cu-Mo mineralization occurs mainly as silicic veins in the syenitic to monzonitic rocks and is composed of chalcopyrite, bornite, molybdenite, enargite, and magnetite as hypogene minerals and covellite, chalcocite, hematite, limonite, malachite, and azurite as supergene minerals (Figures 22-f to h). In general, there are at least two main fault systems in the Lar Cu-Mo mineralization with NW-SE and NE-SW trends. The NW-SE system is mainly associated with mineralization and has been displaced with younger NE-SW system.

CONCLUSİON

Numerous copper deposits are identified by widespread alterations in both mineralized and surrounding rocks of the deposits that are usually formed in tectonized rocks. The tectonized rocks are transmitter of the ore forming hydrothermal fluids. Hydroxyl-bearing and iron oxide minerals are some of the most common minerals in such environments which are useful in the ore mineral exploration.
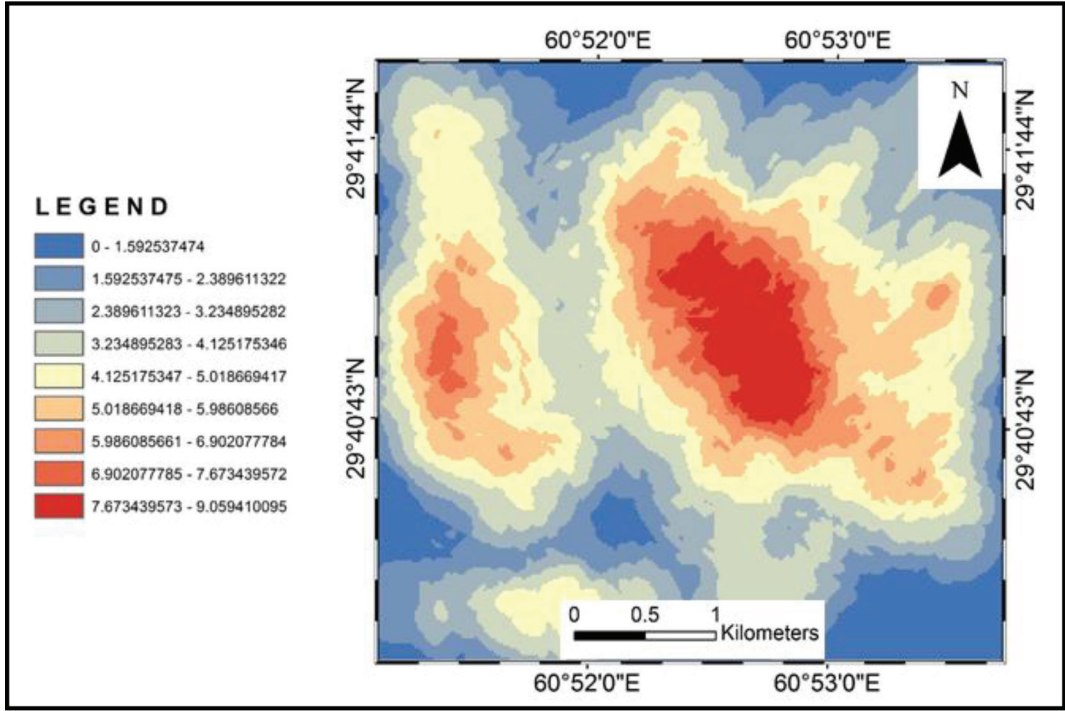
Figure 20. Lineation contour map which represents the maximum compliance between mineralized areas and high values of photolineament factors.
Şekil 20.   Mineralize alanlarla fotoçizgisellik faktörleri arasında en fazla uyumu gösteren çizgisellik kontur haritası.
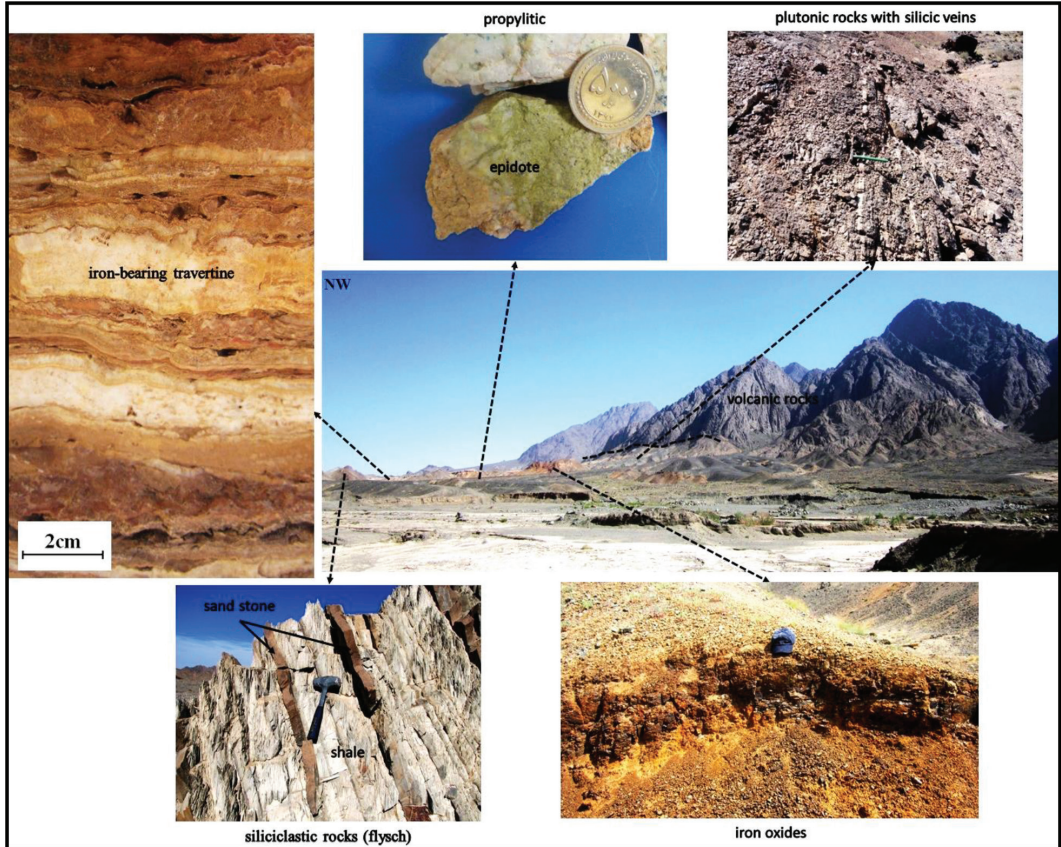

Figure 21. Field photographs of the Lar Cu-Mo mineralization.
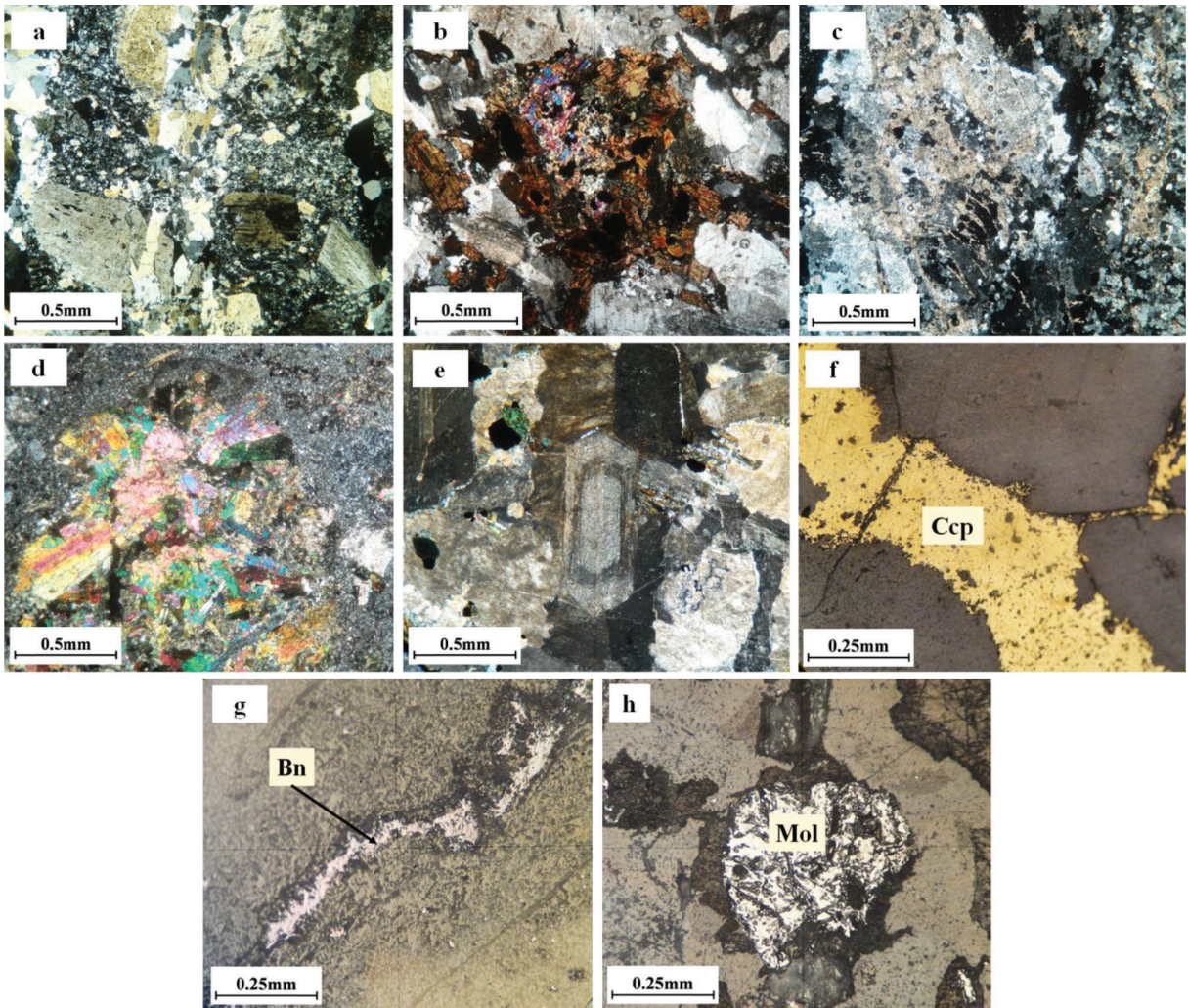*Şekil 21.   Lar Cu-Mo yatağının arazi resimleri.*

Figure 22. Photomicrographs of (a) silicic alteration, (b) potassic alteration, (c) phyllic alteration, (d) propylitic alteration, (e) argillic alteration, (f) chalcopyrite, (g) bornite, (h) molybdenite (Bn: bornite, Ccp: chalcopyrite, Mol: molybdenite).

Şekil 22.   Mikroresimler: a) Silisik bozunma b) Potasik bozunma c) Fillik bozunma d) Propilitik bozunma e) Arjillik bozunma f) Kalkopirit g) Bornit h) Molibdenit (Bn: bornit, Ccp: kalkopirit, Mol: molibdenit).

Since Landsat-8 images are applicable for the study of the alterations, lineaments, and local controller structures of the copper deposits, therefore, we used it to study alterations and lineaments in the Lar Cu-Mo mineralization. The color composite and band ratio methods clearly showed the hydrothermal altered areas in the southwestern part of the Lar igneous complex. Certainly, both LS-Fit and Crosta methods were useful to map spectral signatures of hydrothermal alterations (i.e. clay minerals and iron oxides). The results from high-pass directional filterings and photolineament factor methods illustrate that sufficient correlation can be found between the alterations, geological structures, and intense influential locations of hydrothermal fluids. Therefore, all methods showed high efficiencies for mapping hydrothermal altered areas especially iron-oxide minerals which are in compliance with field observations. Therefore, using different image processing techniques on Landsat-8 images increases the validity of results and also decreases the systematic errors during the field studies in arid and semi-arid areas.

REFERENCES

Abdelsalam, M., and Stern, R., 2000. Mapping gossans in arid regions with Landsat TM and SIR-C images, the Beddaho Alteration Zone in northern Eritrea. Journal of African Earth Sciences. 30, 903-916.

Abrams, M.J., Ashley, R.P., Brown, L.C., Goetz, A.F.H., and Kahle, A.B., 1997. Mapping of hydrothermal alteration in the Cuprite mining district, Nevada, using aircraft scanning images for the spectral region 0.46 to 2.36 mm. Geology. 5, 713–718.

Ali, A., and Pour, A., 2014. Lithological mapping and hydrothermal alteration using Landsat 8 data: A case study in Ariab mining district, Red Sea Hills, Sudan. International Journal of Basic and Applied Sciences. 3, 199–208.

Amer, R., Kusky, T., and Ghulam, A., 2010. Lithological mapping in the central eastern desert of Egypt using ASTER data. Journal of African Earth Sciences. 56, 75–82.

Bagheri, S., and Bakhshi, M.R., 2001. Investigation of north Zahedan magmatism and its relation to ore genesis. Published Research Report. University of Sistan and Baluchestan.

Behrouzi, A., 1993. Geological map of Zahedan quadrangle (1:250000). Geological Survey of Iran.

Bennett, S.A., Atkinson, W.W., and Kruse, F.A., 1993. Use of Thematic Mapper imagery to identify mineralization in the Santa Teresa district, Sonara, Mexico. International Geology Review. 35, 1009–1029.

Berberian, M., and King, G.C.P., 1981. Towards a paleogeography and Tectonic evolution of Iran. Canadian Journal of Earth Sciences. 8, 210–265.

Boomeri, M., 2004. Mineralogy and geochemistry of Lar mountains igneous rocks in northern part of Zahedan. 12th Symposium of Crystallography and Mineralogy of Iran.

Boomeri, M., Lashkaripour, G.R., and Gorgij, M.N., 2005. F and Cl in biotites from Zahedan granitic rocks. Iranian Journal of Crystallography and Mineralogy. 13, 79-94.

Camp, V.E., and Griffis, R.J., 1982. Character, genesis and tectonic setting of igneous rocks in the Sistan Suture Zone, eastern Iran. Lithos. 15, 221-239.

Carranza, E.J.M., and Hale, M., 2002 Mineral imaging with Landsat Thematic Mapper data for hydrothermal alteration mapping in heavily vegetated terrane. International Journal of Remote Sensing. 23, 4827–4852.

Chance, P., 1981. Petrogenesis of a low-Ti, potassic suite: Kuh-e Lar caldera subsidence complex, eastern Iran. MSc Thesis. University of Western Ontario.

Ciampalini, A., Garfagnoli, F., Antonielli, B., Moretti, S., and Righini, G., 2013a. Remote sensing techniques using Landsat ETM+ applied to the detection of iron ore deposits in Western Africa. Arabian Journal of Geosciences. 6, 4529–4546.

Crosta, A., and Moore, J., 1989. Enhancement of Landsat Thematic Mapper imagery for residual soil mapping in SW Minas Gerais State, Brazil: A prospecting case history in Greenstone belt terrain; International Proceedings of the Seventh Erim Thematic Conference: Remote Sensing for Exploration Geology, 1173–1187.

Crosta, A.P., Souza Filho, C.R., Azevedo, F., and Brodie, C., 2003. Targeting key alteration minerals in epithermal deposits in Patagonia, Argentina, using ASTER imagery and principal component analysis. International Journal of Remote Sensing. 24, 4233–4240.

Daneshfar, B., Desrochers, A., and Budkewitsch, P., 2006. Mineral-potential mapping for MVT deposits with limited data sets using Landsat data and geological evidence in the Borden Basin, Northern Baffin Island, Nunavut, Canada. Natural Resources Research. 15, 129–149.

Di Tommaso, I., and Rubinstein, N., 2007. Hydrothermal alteration mapping using ASTER data in the Infiernillo porphyry deposit, Argentina. Ore Geology Reviews. 32, 275–290.

Drury, S., 2001. Image Interpretation in Geology (p. 290). Cheltenham Malden: Nelson Thornes Blackwell Science.

Ducart, D.F., Silva , A.M., Toledo, C.L.B., and de Assis, L.M., 2016. Mapeamento de óxidos de ferro usando imagens Landsat-8/OLI e EO-1/Hyperion nos depósitos ferríferos da Serra Norte, Província Mineral de Carajás, Brasil. Brazilian Journal of Geology. 46, 331-349.

Farhoudi, G., and Karig, D.E., 1977. Makran of Iran and Pakistan as an active arc system. Geology. 5, 664-668.

Farokh-Nezhad, M., 2011. Geochemical characterization of potassic mafic rocks, monzonites and syenites from Lar complex, eastern Iran. MSc Thesis. University of Sistan and Baluchestan.

Gahlan, H., and Ghrefat, H., 2017. Detection of gossan zones in arid regions using Landsat-8 OLI data: implication for mineral exploration in the eastern Arabian shield, Saudi Arabia. Natural Resources Research, 1-16.

Ghafari-Bijar, S., 2009. Geochemistry of potassic mafic rocks in the Lar complex, north of Zahedan, east of Iran. MSc Thesis. University of Sistan and Baluchestan.

Ghasemi, H., Sadeghian, M., Kord, M., and Khanalizadeh, A., 2010. The evolution mechanisms of Zahedan granitoidic batholith, southeast Iran. Iranian Journal of Crystallography and Mineralogy. 17, 551-578.

Goetz, A.F., Rock, B.N., and Rowan, L., 1983. Remote sensing for exploration: an overview. Economic Geology. 78, 573–590.

Gupta, R.P., 2003. Remote Sensing Geology, Heidelberg, Springer.

Haghipour, A., Saidi, A., Aganabati, A., Moosavi, A., Mohebi, A., Sadeghi, M., and et al., 2009. International geological map of the Middle East (1:5,000,000). Second ed. Geological Survey of Iran.

Hardcastle, K.C., 1995. Photolineament Factor: A new computer-aided method for remotely sensing the degree to which bedrock is fractured. Photogrammetric Engineering and Remote Sensing. 61, 739-747.

Haroni, H.A., and Lavafan, A., 2007. Integrated analysis of Aster and Landsat Etm data to map exploration targets in the Muteh gold-mining area, Iran. Available at: http://www.itc.nl/issdq/accessed 20 June 2009.

Hosseini, M.R., 2002. Petrology and geochemistry of SW-Zahedan granitoids. MSc Thesis. University of Tehran.

Kan Iran Engineering., 1999. Report of the Lar copper deposit geological map. Tehran. Iran. National Iranian Copper Industries Co (NICICO).

Karimi, A., 2002. Geochemical behaviors and geological studies of copper and paragenesis elements in Lar prospect (North Zahedan).

Geosciences Scientific Quarterly Journal. 43, 56-67.

Kaufman, H., 1988. Mineral exploration along the Agaba–Levant structure by use of TM-data concepts, processing and results. International Journal of Remote Sensing. 9, 1630–1658.

Kord, M., 2005. Petrology and geochemistry of Cheshme Bid granitoids, southeast of Zahedan. MSc Thesis. Shahrood University of Technology.

Loughlin, W.P., 1991. Principal component analysis for alteration mapping. Photogrammetric Engineering and Remote Sensing. 57, 1163–1169.

Madani, A.M., 2009. Utilization of Landsat ETM+ data for mapping gossans and iron rich zones exposed at Bahrah area, western Arabian Shield, Saudi Arabia. Journal of King Abdulaziz University, Earth Sciences. 20, 35–49.

Masoumi, F., Eslamkish T., Honarmand, M., and Abkar, A.A., 2017. A Comparative Study of Landsat-7 and Landsat-8 Data Using Image Processing Methods for Hydrothermal Alteration Mapping. Resource Geology. 67, 72-88.

Mohammadi, A., Burg, J.P., Bouilhol, P., and Ruh, J., 2016. U–Pb Geochronology and Geochemistry of Zahedan and Shah Kuh Plutons, Southeast Iran: Implication for Closure of the South Sistan Suture Zone, Lithos 248–251, 293–308.

Moores, E.M., and Twiss, R.J., 1995. Tectonics, Freeman, New York.

Moradi, R., Boomeri, M., and Bagheri, S., 2014. Petrography and geochemistry of intrusive rocks in the Shurchah antimony-bearing area Southeast of Zahedan. Journal of Petrology (Isfahan University). 5, 15-32.

Nakisa, M., 2002. Results of Exploration Studies and Reserves Estimation of the Lar Cu Ore Deposit-Zahedan. Tehran, Iran, Ministry of Industries and Mines, National Iranian Copper Industries Co.

Pour, B.A., and Hashim, M., 2011a. Identification of hydrothermal alteration minerals for exploring of porphyry copper deposit using ASTER data, SE Iran. Journal of Asian Earth Sciences. 42, 1309-1323.

Pour, B.A., and Hashim, M., 2011b. Application of Spaceborne Thermal Emission and Reflection Radiometer (ASTER) data in geological mapping. International Journal of Remote Sensing. 6, 7657-7668.

Pour, B.A., and Hashim, M., 2012a. The application of ASTER remote sensing data to porphyry copper and epithermal gold deposits. Ore Geology Reviews. 44, 1-9.

Pour, B.A., and Hashim, M., 2012b. Identifying areas of high economic-potential copper mineralization using ASTER data in Urumieh-Dokhtar Volcanic Belt, Iran. Advances in Space Research. 49, 753-769.

Pour, B.A., and Hashim, M., 2013. Fusing ASTER, ALI and Hyperion data for enhanced mineral mapping. International Journal of Image and Data Fusion. 4, 126-145.

Pour, B.A., and Hashim, M., 2014. ASTER, ALI and Hyperion sensors data for lithological mapping and ore minerals exploration. Springerplus. 3, 130.

Pour, B.A., and Hashim, M., 2015a. Evaluation of Earth Observing-1 (EO1) Data for Lithological and Hydrothermal Alteration Mapping: A Case Study from Urumieh-Dokhtar Volcanic Belt, SE Iran. Journal of the Indian Society of Remote Sensing. 43, 583-597.

Pour, B.A., and Hashim, M., 2015b. Integrating PALSAR and ASTER data for mineral deposits exploration in tropical environments: a case study from Central Belt, Peninsular Malaysia. International Journal of Image and Data Fusion. 6, 170-188.

Pour, A.B., and Hashim, M., 2015c. Hydrothermal alteration mapping from Landsat-8 data, Sar Cheshmeh copper mining district, southeastern Islamic Republic of Iran. Journal of Taibah University for Science. 9, 155-166.

Pour, B.A., Hashim, M., and Marghany, M., 2014. Exploration of gold mineralization in a tropical region using Earth Observing-1 (EO1) and JERS-1 SAR data: a case study from Bau gold field, Sarawak, Malaysia. Arabian Journal of Geosciences. 7, 2393-2406.

Rahnama-Rad, J., Sahebzadeh, B., and Mirhajizadeh, A.A., 2008. Weathering and weakness of Zahedan granitoids: a rock engineering point of view. Applied Geology. 4, 247-257.

Ranjbar, H., Honarmand, M., and Moezifar, Z., 2004. Application of the Crosta technique for porphyry copper alteration mapping, using ETM+ data in the southern part of the Iranian volcanic sedimentary belt. Journal of Asian Earth Sciences. 24, 237–243.

Rowan, L.C., Goetz, A.F., and Ashley, R.P., 1977. Discrimination of hydrothermally altered and unaltered rocks in visible and near infrared multispectral images. Geophysics. 42, 522–535.

Sabins, F.F., 1997. Remote Sensing-Principles and Interpretation, third ed. W.H. Freeman and Co, New York.

Sabins, F.F., 1999. Remote sensing for mineral exploration. Ore Geology Reviews. 14, 157–183.

Sadeghian, M., 2005. Magmatism, metallogeny and emplacement mechanisms of Zahedan granitoidic pluton. PhD Thesis. University of Tehran.

Sadeghian, M., Bouchez, J.L., Ne de lec, A., Siqueira, R., and Valizadeh, M.V., 2005. The granite pluton of Zahedan (southeast of Iran): a petrological and magnetic fabric study of a syntectonic sill emplaced in a transtensional setting. Journal of Asian Earth Sciences. 25, 301-327.

Sadeghian, M., and Valizadeh, M.V., 2007. Emplacement mechanism of Zahedan granitoidic pluton with the aid of AMS method. Earth Sciences. 17, 126-143.

Safari, M., Maghsoudi, A., and Pour, A.B., 2017. Application of Landsat-8 and ASTER satellite remote sensing data for porphyry copper exploration: a case study from Shahr-e-Babak, Kerman, south of Iran. Geocarto International, 1-16.

Sahebzadeh, B., 1996. Petrography and petrology of igneous intrusive of Zahedan-Lochan. MSc Thesis. Islamic Azad University.

Shalaby, M.H., Bishta, A.Z., Roz, M.E., and Zalaky, M.A., 2010. Integration of geologic and remote sensing studies for the discovery of uranium mineralization in some granite plutons, Eastern Desert, Egypt. Journal of King Abdulaziz University, Earth Sciences. 21, 1–25.

Soltanian, A., 2013. Petrogenesis of volcanic rocks from Lar complex, north of Zahedan, east of

Iran. MSc Thesis. University of Sistan and Baluchestan.

Tangestani, M.H., and Moore, F., 2001. Comparison of three principal component analysis techniques to porphyry copper alteration mapping: a case study, Meiduk area, Kerman, Iran. Canadian Journal of Remote Sensing. 27, 176–181.

Thurmond, A., Abdelsalam, M., and Thurmond, J., 2006. Optical-radar- DEM remote sensing data integration for geological mapping in the afar depression, Ethiopia. Journal of African Earth Sciences. 44, 119–134.

US Geological Survey., 2012. Landsat Data Continuity Mission. US Geological Survey, Washington, DC.

Wester, K., 1992. Spectral signature measurements and image processing for geological remote sensing. PhD Thesis. Department of Physical Geography. Stockholm University. Stockholm.

Zhang, T., Yi, G., Li, H., Wang, Z., Tang, J., Zhong, K., Li, Y., Wang, Q., and Bie, X., 2016. Integrating Data of ASTER and Landsat-8 OLI (AO) for Hydrothermal Alteration Mineral Mapping in Duolong Porphyry Cu-Au Deposit, Tibetan Plateau, China. Remote Sensing. 8, 1-23